HHS Public Access

Author manuscript

Nat Cell Biol. Author manuscript; available in PMC 2016 March 01.

Published in final edited form as:

Nat Cell Biol. 2015 September ; 17(9): 1099–1111. doi:10.1038/ncb3217.

Distinct Regulatory Mechanisms Govern Embryonic versus Adult Adipocyte Maturation

Qiong A. Wang[1], **Caroline Tao**[1], **Lei Jiang**[2], **Mengle Shao**[1], **Risheng Ye**[1], **Yi Zhu**[1,3], **Ruth Gordillo**[1], **Aktar Ali**[1], **Yun Lian**[4], **William L. Holland**[1], **Rana K. Gupta**[1], and **Philipp E. Scherer**[1,5,*]

[1]Touchstone Diabetes Center, Department of Internal Medicine, University of Texas Southwestern Medical Center, Dallas, Texas 75390, USA

[2]Children's Medical Center Research Institute, University of Texas Southwestern Medical Center, Dallas, Texas 75390, USA

[3]LIFA Diabetes, Lilly Research Laboratories, Division of Eli Lilly and Company, Indianapolis, Indiana 46285, USA

[4]Center for Immunology, University of Texas Southwestern Medical Center, Dallas, Texas 75390, USA

[5]Department of Cell Biology, University of Texas Southwestern Medical Center, Dallas, Texas 75390, USA

Abstract

Pathological expansion of adipose tissue contributes to the metabolic syndrome. Distinct depots develop at various times under different physiological conditions. The transcriptional cascade mediating adipogenesis is established *in vitro*, and centers around a core program involving PPARγ and C/EBPα. We developed an inducible, adipocyte-specific knockout system to probe the requirement of key adipogenic transcription factors at various stages of adipogenesis *in vivo*. C/EBPα is essential for all white adipogenic conditions in the adult stage, such as adipose tissue regeneration, adipogenesis in muscle and unhealthy expansion of white adipose tissue during high fat feeding or due to leptin deficiency. Surprisingly, terminal embryonic adipogenesis is fully C/EBPα independent, does depend however on PPARγ; cold-induced beige adipogenesis is also C/EBPα independent. Moreover, C/EBPα is not vital for adipocyte survival in the adult stage. We reveal a surprising diversity of transcriptional signals required at different stages of adipogenesis *in vivo*.

*Correspondence should be addressed to: Philipp E. Scherer, Touchstone Diabetes Center, Department of Internal Medicine, University of Texas Southwestern Medical Center, 5323 Harry Hines Blvd., Dallas, TX, 75390-8549, USA, Philipp.Scherer@utsouthwestern.edu, Tel: 214-648-8715, Fax: 214-648-8720.

Author Contributions

Q.A.W., R.K.G. and P.E.S designed the experiments and wrote the manuscript. Q.A.W., C.T., L.J., M.S., R.Y., Y.Z., R.G., A.A., R.K.G. performed experiments and analyzed data. Y. L. and W.L.H. analyzed data.

Introduction

White adipose tissue (WAT) has been recognized as a major endocrine organ that is highly dynamic and metabolically active[1–3]. Adipocytes from anatomically distinct adipose tissues have unique functions and contribute differentially to whole body insulin resistance, dyslipidemia, chronic inflammation, and numerous other metabolic disorders[4–7]. There are two phases of adipogenesis: commitment of multipotent stem cells to the pre-adipocyte lineage and terminal differentiation of pre-adipocytes to mature adipocytes[8]. Furthermore, mechanisms must be in place to maintain the function and terminally differentiated state of the adipocyte. The transcriptional cascade driving adipogenesis has been extensively studied in cellular models of adipogenesis, such as the murine 3T3-L1 cell line, primary stromal-vascular derived cells or mouse embryonic fibroblasts (MEFs)[8–10]. Elegant work in 3T3-L1 cells has defined key transcription factors that are essential for the commitment of pre-adipocytes to undergo maturation *in vitro*[11, 12]. At the center of this transcriptional network is the nuclear hormone receptor PPARγ, which serves as the "master regulator" of adipogenesis, as well as C/EBPα, the founding member of the CCAAT/enhancer-binding family. Numerous additional transcriptional regulators have been implicated in adipogenesis; however, the duo of PPARγ and C/EBPα has been widely viewed as "core" regulators of all forms of adipogenesis. Moreover, genome-wide analyses of promoter architecture has revealed that PPARγ and C/EBPα co-occupy and regulate a large portion of the global adipocyte transcriptome *in vitro*, suggesting that these two factors coordinate the maintenance of the adipocyte morphology and function[13, 14].

Adipogenesis *in vivo* is governed by a more complex set of events than in a tissue culture setting[15–18], when and where these specific factors drive the development and expansion of fat pads *in vivo* cannot be determined in the *in vitro* system[19]. To better understand the dynamics of adipogenesis in different locations and under different physiological conditions, we developed a doxycycline-inducible adipocyte-specific knockout system that is active during late adipocyte maturation and/or in mature adipocytes. This system enables us to explore the role of specific components of the adipogenic transcriptional machinery in different locations and under different conditions of late stage adipogenesis *in vivo*, as well as their role in terminally differentiated adipocytes. In this study, we focused predominantly on the transcription factor C/EBPα as a tool to address the question how the loss of C/EBPα function during adipocyte maturation affects adipocyte maturation and maintenance in different fat depots in response to developmental and nutritional conditions. Our results show that the transcriptional signals needed during adipocyte maturation are highly diverse within the same depot at different times of lifespan and under different conditions of adipogenesis.

Results

Adipocyte specific inducible knockout of C/EBPα

To achieve an inducible knockout of C/EBPα in adipocytes, we crossed three mouse lines: an adiponectin promoter-driven "tet-on" transcription factor rtTA (Adn-rtTA) line we recently generated[20, 21], a tet-responsive CRE (TRE-Cre) line[22], and the conditional C/EBPα$^{flox/flox}$ line[23]. In the absence of doxycycline, C/EBPα is expressed normally in all

cells (Adn-C/EBPα$^{flox/flox}$). Upon treatment with doxycycline, rtTA activates the TRE promoter to induce Cre expression. Cre protein will subsequently eliminate the floxed region in the C/EBPα locus and permanently inactivate C/EBPα in adiponectin promoter active cells (Adn-C/EBPα$^{-/-}$) (Supplementary Fig. 1a). Starting at 10 weeks of age, upon full development of all white adipose tissues (WAT), Adn-C/EBPα$^{flox/flox}$ mice were put on doxycycline-containing chow diet. One week of doxycycline treatment dramatically reduced *C/EBPα* mRNA expression levels in subcutaneous adipose tissue (sWAT), epididymal adipose tissue (eWAT), and brown adipose tissue (BAT) of Adn-C/EBPα$^{-/-}$ mice, compared to their control littermates (mice carrying only TRE-Cre and C/EBPα$^{flox/flox}$ or only Adn-rtTA and C/EBPα$^{flox/flox}$) (Supplementary Fig. 1a), while *C/EBPα* expression in other tissues was not altered (Supplementary Fig. 1b). We then separated adipocytes from the stromal vascular fraction (SVF) and a significant drop of *C/EBPα* mRNA levels was observed in the floated adipocytes from sWAT and eWAT, while comparable *C/EBPα* expression levels were seen in the SVFs (Supplementary Fig. 1c), indicating that the C/EBPα knockout is adipocyte specific. The mRNA levels of *C/EBPβ*[24, 25], in contrast, were not altered after C/EBPα elimination (Supplementary Fig. 1c), indicating that the decrease of C/EBPα in adipocytes has no impact on *C/EBPβ* expression. Protein levels of C/EBPα were also reduced dramatically in the sWAT and eWAT after 4 days of doxycycline chow diet treatment, while C/EBPα in the liver was not altered (Supplementary Fig. 1d). We next isolated and differentiated SVF from sWAT of Adn-C/EBPα$^{flox/flox}$ mice. *C/EBPα* expression was dramatically up-regulated on day one of differentiation and reached its peak by day 2; *PPARγ* expression was greatly up-regulated on day two and reached its peak by day 3 (Supplementary Fig. 1e). *Adiponectin* and *rtTA* mRNA levels are increased only by the 3rd day of differentiation and reached their peak on day 4, when the cells are starting to exhibit a true adipocyte morphology, with visible lipid accumulation revealed by Oil Red O staining (Supplementary Fig. 1f). Thus, adiponectin and rtTA are only activated in the later stages of differentiation, during adipocyte maturation, after C/EBPα and PPARγ start to be induced. To determine whether C/EBPα deficiency alters the binding capacity of C/EBPβ and PPARγ on their target sequences, we performed chromatin immunoprecipitation (CHIP) assays with anti-C/EBPα, C/EBPβ or PPARγ antibodies in differentiated adipocytes obtained upon *in vitro* differentiation of SVF cells from control or Adn-C/EBPα$^{-/-}$ sWAT (Supplementary Fig. 1g). ChIP-qPCR analysis showed that the occupancy of C/EBPα was reduced dramatically on the CD36 and C/EBPβ promoters. Binding of C/EBPβ or PPARγ on CD36 and C/EBPβ promoters were unaltered, indicating that the deletion of C/EBPα does not alter the binding capacity of C/EBPβ or PPARγ (Supplementary Fig. 1g). These results enable us to inducibly eliminate genes during the maturation of adipocytes, not only independent of the formation of adipocyte progenitors, but also independent of the early activation of C/EBPα and PPARγ.

Embryonic adipogenesis depends on PPARγ, but not C/EBPα

C/EBPα is essential for adipogenesis *in vitro*[26, 27], but the cell-autonomous role of C/EBPα in adipogenesis *in vivo* has not yet been clearly demonstrated[28–30]. We first addressed whether C/EBPα is required during the initial wave of adipogenesis during the perinatal period. Our previous AdipoChaser system showed that the development of eWAT in males and parametrial WAT (pWAT) in females is postnatal[31]. In contrast, sWAT differentiation

is initiated during embryonic days (E) 14–18, and the number of adipocytes in sWAT remains quite stable postnatally[31]. In order to knockout C/EBPα in late embryonic development of sWAT, control female mice were mated with male Adn-C/EBPα$^{flox/flox}$ mice. Pregnant female mice were put on doxycycline chow diet from E11 to postnatal day (P) 16 (Adn-C/EBPα$^{-/-}$) (Fig. 1a). As previously shown, Cre expression is completely lost after overnight doxycycline withdrawal[31]; any adipocyte developed *after* P16 expresses C/EBPα, while adipocytes developed *before* P16 do not express C/EBPα. C/EBPα protein levels were almost completely gone in the sWAT of Adn-C/EBPα$^{-/-(E11\text{-}P16)}$ mice, while normal expression is observed in eWAT and liver (Fig. 1b). Immunofluorescence staining further confirmed that C/EBPα is expressed in the adipocyte nucleus in eWAT (Supplementary Fig. 2a), but not sWAT of Adn-C/EBPα$^{-/-(E11\text{-}P16)}$ mice (Supplementary Fig. 2b). Remarkably, both sWAT and eWAT/pWAT tissue mass and average adipocyte size in the adult Adn-C/EBPα$^{-/-(E11\text{-}P16)}$ mice were comparable to their control littermates (Fig. 1c, d and Supplementary Fig. 2c). The average adipocyte numbers per image are: sWAT control group, 358; sWAT Adn-C/EBPα$^{-/-(E11\text{-}P16)}$ group, 445; eWAT control group, 362; eWAT Adn-C/EBPα$^{-/-(E11\text{-}P16)}$ group 324. $n = 2$ image per group. The total number of adipocytes in Adn-C/EBPα$^{-/-(E11\text{-}P16)}$ mice is 101% (sWAT) and 121% (eWAT) of their control littermates. C/EBPα-deficient sWATs also had normal adipocyte morphology by hematoxylin and eosin (H&E) staining (Fig. 1e and Supplementary Fig. 2d). Essentially all adipocytes in sWAT, eWAT and pWAT from Adn-C/EBPα$^{-/-(E11\text{-}P16)}$ mice represent live adipocytes with positve perilipin staining (Fig. 1f and Supplementary Fig. 2e). BAT from these Adn-C/EBPα$^{-/-(E11\text{-}P16)}$ mice also had much reduced C/EBPα protein levels (Supplementary Fig. 2f), but slightly enlarged adipocyte cell size (Supplementary Fig. 2g, h). When mice were put on doxycycline chow diet from P0 to P42, during the critical period of eWAT development (Supplementary Fig. 3a–d), or from E11 to P42, during both sWAT and eWAT development (Supplementary Fig. 3e–g), Adn-C/EBPα$^{-/-}$ mice also had normal sWAT and eWAT tissue mass. This leads us to conclude that C/EBPα is *not* required for the maturation of sWAT during embryogenesis or eWAT during early postnatal development.

PPARγ is necessary and sufficient to induce adipocyte differentiation *in vitro*[9]. We also generated an adipocyte-specific inducible PPARγ knockout model (Adn-PPARγ$^{flox/flox}$) by crossing Adn-rtTA mice with TRE-Cre mice and PPARγ$^{flox/flox}$ mice[32]. The adult Adn-PPARγ$^{-/-(E11\text{-}P16)}$ male offspring (Fig. 1a) had small amounts of sWAT (Fig. 1g). These very small sWAT pads of Adn-PPARγ$^{-/-(E11\text{-}P16)}$ mice have disrupted adipocyte morphology (Fig. 1h), with widespread negative perilipin staining (Fig. 1i). The lack of sWAT enhanced eWAT generation, resulting in increased eWAT mass (by 36%) and increased adipocyte size (Fig. 1g), with normal viability and morphology (Fig. 1h, i). These observations indicate that, in contrast to C/EBPα, deleting PPARγ in the same critical late developmental stages of sWAT totally blocked the formation of sWAT, leading to a compensatory overgrowth of eWAT.

Adipocyte morphology is not maintained by C/EBPα

To determine if adipocytes without C/EBPα are viable *in vitro*, we added doxycycline to fully differentiated adipocyte cultures derived from SVF of sWAT from Adn-C/

EBPα$^{flox/flox}$ or control littermates. C/EBPα expression in Adn-C/EBPα$^{-/-}$ adipocytes was effectively eliminated after 3 days of doxycycline treatment (Fig. 2a). These C/EBPα-deficient adipocyte cultures had a similar density of Oil Red O staining compared to control cultures (Fig. 2b), with positive perilipin (Fig. 2c) and lipid staining (Fig. 2d), *on par* with control adipocytes.

In vivo studies showed that upon putting the Adn-C/EBPα$^{flox/flox}$ mice on a doxycycline chow diet (Fig. 3a), insulin-stimulated phosphorylation of Akt and Erk1/2 was significantly impaired in the sWAT and eWAT (Fig. 3b), but not in the liver (Fig. 3b). These results indicate that C/EBPα in white adipocytes cell-autonomously regulates insulin signaling. Consistent with the *in vitro* observations (Fig. 2c, d), adipocytes in these Adn-C/EBPα$^{-/-}$ mice have relatively normal morphology and adipocyte size distribution (Fig. 3c), indicating these WAT have a comparable number of adipocytes. The average adipocyte numbers per image are sWAT control group, 167; sWAT Adn-C/EBPα$^{-/-}$ group, 209; eWAT control group, 72; eWAT Adn-C/EBPα$^{-/-}$ group 67. n = 2 image per group. Notably, the plasma adiponectin is very sensitive to C/EBPα levels in mature adipocytes. Deletion of C/EBPα led to a rapid decrease of adiponectin in circulation which dropped to 14% of their control littermates after 8 days (Fig. 3d). Interestingly, circulating adiponectin is reduced by 34% in the male Adn-C/EBPα$^{-/-(E11\text{-}P16)}$ mice (Fig. 3e), suggesting that sWAT contributes about one third of the adiponectin in systemic circulation. In Adn-PPARγ$^{-/-(E11\text{-}P16)}$ mice, circulating adiponectin is only reduced by 24% (Fig. 3f), reflecting the fact that the increased eWAT tissue mass compensates by secreting more adiponectin into circulation (Fig. 1g).

C/EBPα transcriptional targets are distinct from PPARγ targets

Our data emphasize that C/EBPα deficiency in mature adipocytes has distinct phenotypic consequences compared to PPARγ deficiency[33–35]. We took a systematic, un-biased approach to determine the direct (acute) transcriptional programs that are specifically dependent on C/EBPα or PPARγ in mature white adipocytes, after doxycycline chow diet feeding for 3 days (Fig. 3g, h and Supplementary Fig. 4). Only 26 genes were significantly changed in C/EBPα deficient fat cells, compared to 298 genes altered when PPARγ is deleted. Surprisingly, only 10 genes were in common between these two target groups (Fig. 3h and Supplementary Fig. 4b). These data indicate that although C/EBPα and PPARγ cross-regulate each other and co-occupy a large common cistrome in the mature adipocyte[13, 14], the distinct global programs directly dependent on each factor *in vivo* are quite distinct.

Adipocyte C/EBPα is essential for glucose/lipid metabolism during HFD feeding

There is much that remains to be learned concerning the role of C/EBPα in maintaining the adipocyte phenotype. The phenotypes described previously are too complicated due to profound effects of deleting C/EBPα in adipocyte progenitors and other cell types[28, 30, 36]. When adult mice were challenged with a doxycycline high fat diet (HFD) (Fig. 4a), Adn-C/EBPα$^{-/-}$ mice still gained body weight, but at a lower rate (Fig. 4b). *In vivo* CT scans and NMR body composition analysis revealed that Adn-C/EBPα$^{-/-}$ mice still have considerable amounts of WAT after 4 weeks of doxycycline HFD feeding (Fig. 4c, d). The differences in

body weights only became significant around 5 weeks after initiation of HFD feeding (Fig. 4b), around the same time that we observed adipogenesis in WAT after hypertrophy[31]. Consistent with the findings in mice on chow doxycycline diet (Fig. 3c), adipocytes in these Adn-C/EBPα$^{-/-}$ mice had relatively normal morphology and average adipocyte size in sWAT, eWAT and BAT (Fig. 4e). The average adipocyte numbers per image are: sWAT HFD control group, 42; sWAT HFD Adn-C/EBPα$^{-/-}$ group, 42; eWAT HFD control group, 41; eWAT HFD Adn-C/EBPα$^{-/-}$ group 43. n = 2 image per group. The total number of adipocytes in HFD Adn-C/EBPα$^{-/-(E11\text{-}P16)}$ mice is 115% (sWAT) and 81% (eWAT) of their HFD control littermates. These adipocytes in Adn-C/EBPα$^{-/-}$ mice are viable with 100% of cells displaying a positive perilipin signal (Fig. 4f). Intraperitoneal glucose tolerance tests (GTT) and insulin tolerance tests (ITT) showed that Adn-C/EBPα$^{-/-}$ mice have impaired glucose tolerance and are more insulin resistant after several weeks of doxycycline HFD feeding (Fig. 4g, h).

The inducible adipocyte-specific C/EBPα deletion also altered whole body lipid metabolism. Triglyceride content of the VLDL fractions of Adn-C/EBPα$^{-/-}$ mice was significantly higher, but cholesterol content of the HDL fractions was unaltered (Supplementary Fig. 5a, b). Meanwhile, Adn-C/EBPα$^{-/-}$ mice had an increased whole body triglyceride clearance rate (Supplementary Fig. 5c). Moreover, the rate of hepatic VLDL-TG production in Adn-C/EBPα$^{-/-}$ mice was almost doubled (Supplementary Fig. 5d). During β-3 adrenergic receptor agonist treatment, Adn-C/EBPα$^{-/-}$ mice showed slightly decreased levels of NEFA and triglyceride in circulation, while glucose levels were significantly increased (Supplementary Fig. 5e–g). Thus, the Adn-C/EBPα$^{-/-}$ mice had increased whole body triglyceride clearance combined with increased hepatic VLDL-TG production. However, hepatic triglyceride and cholesterol levels were not changed in these mice (Supplementary Fig. 5h, i). Metabolic cage studies showed that during week 7 of doxycycline HFD feeding, Adn-C/EBPα$^{-/-}$ mice had significantly higher physical activity (Supplementary Fig. 5j) and oxygen consumption (Supplementary Fig. 5k), with no appreciable alteration in RER and food intake, compared to control littermates (Supplementary Fig. 5l, m).

Ceramide levels positively correlate with impaired glucose tolerance and insulin sensitivity[37], and adiponectin is highly involved in controlling these lipids[38]. We observed a widespread up-regulation in the concentration of sphingoid bases, ceramide and sphingomyelin content in sWAT and eWAT after 1 month of doxycycline HFD feeding (Supplementary Fig. 6a–i). The rapid drop of adiponectin levels in circulation after the induced C/EBPα elimination in WAT (Fig. 3d), combined with our previous studies[38], suggests that C/EBPα is at least partially regulating ceramide metabolism through controlling adiponectin expression. Long-term C/EBPα elimination also altered the expression levels of critical transcription factors, key adipokines and enzymes. 1 month of doxycycline HFD feeding decreased *PPARγ* and *LXRα* (Supplementary Fig. 6j), *adiponectin*, *resistin* and *CD36* (Supplementary Fig. 6k), as well as *SCD-1* and *Elovl6* (Supplementary Fig. 6l).

In order to have a more complete profile of altered gene expression upon C/EBPα deletion, we collected microarray data from sWAT of Adn-C/EBPα$^{-/-}$ mice after 3 days or 1 month

of doxycycline HFD treatment (Supplementary Fig. 4c). This yielded a total of 110 (3 days) and 702 (1 month) genes whose expression was significantly altered (Supplementary Fig. 4d, e). IPA pathway analysis (a comparison across the canonical pathways), comparing the three C/EBPα deletion arrays with the acute PPARγ deletion array on chow diet (Supplementary Table 1–4) showed 3 days post C/EBPα deletion (on either chow or HFD) had no overlap with pathway changes 3 days post PPARγ deletion on chow diet. Interestingly, expression patterns 1 month *post* C/EBPα deletion shared 12 common pathways with 3 days of PPARγ deletion on chow diet (Supplementary Fig. 7). We conclude that compared to the genes identified in Adn-C/EBPα$^{-/-}$ mice on the chow diet, most of the C/EBPα targets in mature adipocytes are genes modulated by long-term HFD feeding, and these targets share significant overlap with the changes observed after acute PPARγ loss on chow diet.

Fat expansion in *ob/ob* mice depends on C/EBPα

We next tested whether C/EBPα is essential for adipose tissue expansion in leptin deficient mice. As soon as *ob/ob* Adn-C/EBPα$^{flox/flox}$ mice were started on the doxycycline treatment (Fig. 5a), these mice stopped gaining additional body weight (Fig. 5b). WAT in the *ob/ob* Adn-C/EBPα$^{-/-}$ mice were much smaller (Supplementary Fig. 8a), after 6 months, sWAT and eWAT of *ob/ob* Adn-C/EBPα$^{-/-}$ mice are less than half of the WAT in their *ob/ob* control littermates (Fig. 5c). Surprisingly, adipocytes in *ob/ob* Adn-C/EBPα$^{-/-}$ mice retained a similar morphology in sWAT, eWAT and BAT, and the average adipocyte size in sWAT and eWAT was not altered (Fig. 5d). The average adipocyte numbers per image are: sWAT, *ob/ob* control group, 86; *ob/ob* Adn-C/EBPα$^{-/-}$ group, 82; eWAT, *ob/ob* control group, 59; *ob/ob* Adn-C/EBPα$^{-/-}$ group, 74. $n = 2$ image per group. Thus, the total number of adipocytes in *ob/ob* Adn-C/EBPα$^{-/-(E11\text{-}P16)}$ mice is 14% (sWAT) and 40% (eWAT) of their *ob/ob* control littermates. These remaining adipocytes in *ob/ob* Adn-C/EBPα$^{-/-}$ mice were 100% positive for perilipin staining (Fig. 5e), indicating that the cells in these depots are live adipocytes, even after prolonged absence of C/EBPα. Liver weights of *ob/ob* Adn-C/EBPα$^{-/-}$ mice were not altered, thus, the ratio of liver weight to total body weight is dramatically higher in the Adn-C/EBPα$^{-/-}$ mice (Fig. 5c), with worse hepatic steatosis (Fig. 5f). Similar to Adn-C/EBPα$^{-/-}$ mice, *ob/ob* Adn-C/EBPα$^{-/-}$ displayed enhanced glucose intolerance (Supplementary Fig. 8b) and higher rate of hepatic VLDL-TG production (Supplementary Fig. 8c). *Ob/ob* Adn-C/EBPα$^{-/-}$ mice also had significantly increased oxygen consumption (Supplementary Fig. 8d), associated with an increase in RER (Supplementary Fig. 8e), indicating the mice are more prone to glucose utilization. *Ob/ob* Adn-C/EBPα$^{-/-}$ mice also displayed slightly increased activity during the night time (Supplementary Fig. 8f). Combined, these observations indicate that deleting C/EBPα both in the context of a HFD as well as in the absence of leptin causes attenuation of adipose tissue expansion and a worsening of insulin resistance and dyslipidemia, represent a typical lipodystrophic model[39].

Our previous study demonstrated that *ob/ob* mice with adiponectin overexpression (*ob/ob* AdTg mice) have significantly enlarged WAT[40]. Here, we crossed the *ob/ob* Adn-C/EBPα$^{flox/flox}$ mice with AdTg mice (Fig. 5a). Surprisingly, these *ob/ob* Adn-C/EBPα$^{flox/flox}$ AdTg mice gained weight at the same rate as the *ob/ob* control littermates (Fig. 5g). The

circulating adiponectin levels dropped dramatically in *ob/ob* Adn-C/EBPα$^{-/-}$ mice, and adiponectin levels were restored in the *ob/ob* Adn-C/EBPα$^{-/-}$ AdTg mice (Fig. 5h). Glucose intolerance, on the other hand, was not restored by adiponectin overexpression (Fig. 5i). WAT mass was preserved in the Adn-C/EBPα$^{-/-}$ AdTg mice (Fig. 5j). These results indicate that by restoring adiponectin in circulation upon C/EBPα deficiency, the associated attenuation of adipose tissue expansion in *ob/ob* mice can be overcome.

Adult white, but not beige adipogenesis depends on C/EBPα

So far, our data has shown that C/EBPα is not required for embryonic white adipogenesis, but critical for adipose tissue expansion during HFD or in leptin deficient mice. Here, we generated a more direct model to study the role of C/EBPα in adult adipogenesis *in vivo*, by crossing the inducible C/EBPα knockout system with our previously characterized FAT-ATTAC mice (*F*AT *A*poptosis *T*hrough *T*riggered *A*ctivation of *C*aspase-8)[41] to obtain FAT-ATTAC/Adn-C/EBPα$^{flox/flox}$ mice (Fig. 6a). The FAT-ATTAC mice carry a transgene encoding a caspase 8 protein fused to a dimerization domain under the control of the aP2 adipocytes–specific promoter. The Adipocytes in FAT-ATTAC/Adn-C/EBPα$^{flox/flox}$ mice were alive with positive perilipin staining prior to dimerization (Fig. 6b). Upon a single treatment with dimerizer, apoptosis is initiated in every adipocyte. 7 days after dimerization, sWAT and eWAT sizes were dramatically reduced (Fig. 6c) and adipocytes were uniformly dead, with disrupted morphology and negative perilipin signal (Fig. 6b). By the 4th week post dimerization, both sWAT and eWAT recovered to around half of their original tissue mass in FAT-ATTAC/Adn-C/EBPα$^{flox/flox}$ mice kept on chow diet (Fig. 6d). These mice displayed ~100% perilipin positive adipocytes 6 week post dimerization (Fig. 6b), suggesting active *de novo* adipogenesis during the recovery stage. The FAT-ATTAC/Adn-C/EBPα$^{-/-}$ mice kept on doxycycline chow diet for 6 weeks post dimerization continued to display a disrupted morphology, with predominantly negative perilipin staining in both sWAT and eWAT (Fig. 6b). By week 4 of recovery post dimerization, FAT-ATTAC/Adn-C/EBPα$^{-/-}$ mice kept on doxycycline chow diet had smaller fat pads after dimerization, compared to FAT-ATTAC/Adn-C/EBPα$^{flox/flox}$ mice kept on chow diet (Fig. 6d). These results indicate that new adipocytes cannot effectively form during the recovery stage without the presence of C/EBPα.

Adipogenesis also occurs within skeletal muscle after injury. After glycerol-induced injury, fibrous tissue is generated around the injection area, and white adipocytes are gradually generated at the site of injury[42]. We tested whether C/EBPα is required for adipogenesis in muscle(Fig. 6e). 3 weeks post-injection, muscle from Adn-C/EBPα$^{-/-}$ mice showed only fibrous tissue but no adipocytes, while muscle from the control littermates showed visible adipocytes (Fig. 6f). In control mice, mRNA of adipocyte markers, such as *adipsin* and *adiponectin*, were all dramatically increased in the glycerol-injected side compared to the PBS injected side (Fig. 6g). *Adipsin* and *adiponectin* expression in the glycerol-injected side of Adn-C/EBPα$^{-/-}$ mice were comparable to the PBS injected side of control mice, but far below the values for the glycerol-injected side of control mice (Fig. 6g). This indicates that the muscle injury-induced adipogenesis in adult mice also critically depends on the presence of C/EBPα.

We have previously found that beige adipocytes induced by cold exposure arise from *de novo* adipogenesis[31]. We determined whether C/EBPα is essential for beigeing of WAT (Fig. 7a). Surprisingly, 10 days after cold exposure, expressions of the beige adipocyte markers *Ucp1* and *Tmem26* in Adn-C/EBPα$^{-/-}$ mice were normal (Fig. 7b). Both control and Adn-C/EBPα$^{-/-}$ mice showed massive browning morphology in sWAT (Fig. 7c). with positive UCP1 staining (Fig. 7d). This distinct absence of the requirement for C/EBPα in this process indicates that although C/EBPα is indispensable for white adipogenesis in adult mice, beige adipogenesis is a unique process that differs from white adipogenesis in the adult that does not require C/EBPα at all.

Discussion

Our study reveals that white adipogenesis in adult mice utilizes distinct mechanisms during embryonic development or beige adipogenesis (Fig. 8). One of our most important results presented here is that the precursor cells giving rise to adipocytes during embryogenesis are different from the precursor cells giving rise to adipocytes in the mature animal, at least as far as the requirements for C/EBPα are concerned. We have tested the requirements of C/EBPα under a number of different adipogenic occasions in adult mice, and the results were quite clear: adipocyte maturation cannot happen while deleting C/EBPα during late white adipogenesis in adult mice under many conditions. In the FAT-ATTAC model, the transgene encoding the caspase 8 fusion protein of FAT-ATTAC mice is under the control of the aP2 promoter, which has been shown to be active in other cell types. The lack of specificity of this aP2 promoter cassette may cause irreversible changes in whole body metabolism. However, our initial characterization of the FAT-ATTAC transgene neither revealed significant expression nor did it cause apoptosis in any of these other cell types. Since WAT effectively regenerates *post* dimerzation, we believe that adipocyte precursors are not affected or eliminated by the transgene.

Beige adipogenesis occurs within sWAT after cold exposure, and arises from *de novo* adipogenesis and is believed to originate from unique precursor cells[43–45]. We have previously shown that rtTA is expressed in the beige cells in AdipoChaser mice[31]. In this study, we found that deleting C/EBPα during beige adipogenesis has no impact on the formation and function of beige adipocytes. These results indicate that C/EBPα expression in the maturation stage is only essential for white adipogenesis in the adult, not for beige adipogenesis or embryonic adipogenesis. We appreciate that sWAT and eWAT have distinct morphology and functions, and these two fat depots may have unique precursor pools, responding to differential developmental and nutritional cues[46–50]. Here, we show a differential temporal requirement for C/EBPα for adipogenesis within the same fat depot.

We have also tested the loss of function of PPARγ under all adult adipogenesis conditions that we have examined for C/EBPα, using the Adn-PPARγ$^{flox/flox}$ model. In general, PPARγ is required in the adult mouse under all conditions that require adipogenesis. However, in contrast to C/EBPα, PPARγ is also required for the survival of mature adipocytes. Upon inducible PPARγ deletion, the overall structure and viability of the fat pad is negatively affected, which is consistent with a recent publication by the group of Lazar[33]. It is difficult to assess *de novo* adipogenesis under these conditions.

Adiponectin is known to be regulated by C/EBPα[51–53]. In our inducible knockout system, adiponectin levels were reduced dramatically after as little as two days of C/EBPα deletion, i.e. one of the earliest read-outs of C/EBPα deficiency. The systemic loss of adiponectin also argues that we systematically eliminate C/EBPα in all fat pads. We were surprised that adiponectin overexpression in the *ob/ob* background can rescue the attenuation of WAT expansion due to C/EBPα deficiency.

Although adiponectin is not required for WAT formation both *in vitro* and *in vivo*[54], it is unknown how adiponectin is involved in WAT expansion and regeneration in adult mice, especially when mice are facing metabolic challenges. Our previous results indicated that adiponectin is highly correlated with healthy expansion of WAT, as well as whole body lipid and glucose metabolism[40, 55–59]. Here, we show that a simple increase of adiponectin can restore adipogenesis in adult mice in the absence of C/EBPα, indicating yet again that the process of adipogenesis shares different mechanisms at different stages of an individual's life. This result also highlights that adiponectin not only controls adipocyte function, it may also directly control adipogenesis under certain conditions.

In vitro studies have shown that most genes induced in adipogenesis are targets for both PPARγ and C/EBPα[13, 14]. However, here we demonstrate that PPARγ and C/EBPα control distinct transcriptional programs with very limited overlap *in vivo*. This observation indicates that C/EBPα is distinct from PPARγ in regulating the function of mature adipocytes, at the level of direct targets under healthy conditions. Not surprisingly, there is a notable lack of phenotypic changes in C/EBPα deficient mice kept on a chow diet. When kept on HFD for 1 month, the C/EBPα-specific transcriptional programs are visible at a much broader range in sWAT, and these programs begin to overlap with acute PPARγ-specific transcriptional programs, suggesting C/EBPα is regulating mostly pathways modulated by high dietary fat exposure. This in turn is consistent with the fact that C/EBPα elimination in the WAT of mice kept on HFD resulted in rapid dysfunction of glucose and lipid metabolism.

Methods

Mice

Mice were maintained in a 12 h dark/light cycle and housed in groups of three to five with unlimited access to water and food (chow diet, number 5058, lab diet, St. Louis, MO; New Brunswick, NJ; doxycycline chow diet (600 mg/kg), S4107, Bio-Serv, Flemington, NJ; doxycycline high fat diet (600 mg/kg), S5867, Bio-Serv as indicated in individual experiments). All mice were on C57BL/6J background. The Adn-rtTA, AdTg and FAT-ATTAC mouse was generated by our lab. TRE-Cre, C/EBPα$^{flox/flox}$, PPARγ$^{flox/flox}$ and *ob/ob* lines were obtained from the Jackson Laboratories. The Institutional Animal Care and Use Committee of the University of Texas Southwestern Medical Center, Dallas, have approved all animal experiments.

Metabolic cage studies were performed in the UTSW Metabolic Core facility. GTTs were performed in mice without access to food for 4 hours prior to administration of 2 g/kg body weight glucose by intraperitoneal injection. ITTs were performed in mice without access to

food for 4 hours prior to administration of 0.75 U/kg body weight insulin (Eli Lilly, Indianapolis, Indiana, USA) by intraperitoneal injection. For triglyceride clearance, mice were fasted overnight and then given 10 μl of intralipid 10 μl/gram body weight by gastric gavage. Approximately 20 μl of blood was collected at the indicated time points. Serum or plasma glucose values were measured with a glucose assay (Sigma, St. Louis, Mo). For β-3 adrenergic receptor agonist tests, blood samples were obtained before and 15, 30, 60 and 120 min after intraperitoneal injection of 1 mg/kg CL316, 243 (Sigma, St. Louis, Mo). Adiponectin was measured with mouse adiponectin ELISA kit (Millipore, Bedford, MA). Serum or plasma triglyceride and cholesterol were measured with an Infinity Triglyceride Kit and Infinity Cholesterol Kit (Thermo Electron Corporation, Vantaa, Finland), respectively. Serum or plasma NEFAs were measured with a NEFA-HR kit (Wako Diagnostics, Mountain View, CA). For histology, adipose or liver tissues (n = 2–3 male mice) were excised and fixed in 10% PBS-buffered formalin overnight. Following paraffin embedding and sectioning, tissues were stained with Hematoxylin and eosin stain (H&E).

SVF Culture and Adipocyte Differentiation

SVF fractions from sWAT were obtained from 5 weeks old male mice of each genotype as indicated. Briefly, dissected sWAT from two mice of each genotype were digested for 1 hour at 37 degree in PBS containing 10 mM $CaCl_2$, 2.4 units/mL dispase II (Roche Diagnostics Corporation, Indianapolis, IN) and 1.5 units/mL collagenase D (Roche Diagnostics Corporation, Indianapolis, IN). Digested cell/tissue mixture was filtered through a 100 μm cell strainer to remove undigested tissues. The flow-through cells was centrifuged for 5 minutes at 600×g at 4°C. Cell pellet was resuspended in complete SVF culture medium (DMEM/F12 Invitrogen, Carlsbad, CA; plus Glutamax, Pen/Strep, and 10% FBS) and then filtered through a 40 μM cell strainer to remove clumps and large adipocytes. The flow-through was centrifuged for 5 minutes at 600 g at 4°C, SVF pellet was then resuspended in complete SVF culture medium and plated onto a 6-well tissue culture plate for RNA extraction and Oil Red O staining, or 35-mm glass bottom tissue culture dish for Immunofluorescence staining. For adipocyte differentiation, cells were exposed to the adipogenic cocktail containing dexamethasone (1 μM), insulin (5 μg/ml), isobutylmethylxanthine (0.5 mM) (DMI) and rosiglitazone (1 μM) in complete SVF culture medium. Forty-eight hours after induction, cells were maintained in SVF culture medium containing insulin (5 μg/ml) and rosiglitazone (1 μM) until harvest. For Oil Red O staining, differentiated adipocytes were fixed by 1 mL of 10% formalin per well for 30 minutes. Following fixation, adipocytes were washed by DI water, and then incubated with 1.5 mL isopropanol for 5 minutes. 1.5 mL Oil Red O working solution (Oil Red O 2 g/L, 60% isopropanol, 40% H_2O) were added to each well for 5 minutes. Finally, each well was washed by tap water until the water rinses off clear.

Quantitative real-time RT-PCR

Total RNA from mouse tissues was isolated using RNeasy Mini Kit (Qiagen, Venlo, Netherlands). First-strand cDNA was synthesized with M-MLV reverse transcriptase and random hexamer primers (Invitrogen, Carlsbad, CA) from 1 μg of RNA. Real-time quantitative PCR was done with the SYBR Green PCR system (Applied Biosystems, Foster

City, CA), using β-actin as an internal control for normalization. All primer sequences are provided in Supplementary Table 5.

Antibodies and Western blot analysis

For western blot analysis of adiponectin, serum samples (n = 2 male mice) were diluted in PBS plus sample loading buffer followed by boiling for 10 min at 95°C. For western blot analysis of tissue samples (n = 2–3 male mice), proteins were extracted in RIPA buffer. Samples were loaded on a Criterion precast gel (Bio-Rad, Hercules, CA), and after SDS-PAGE the samples were subjected to immunoblot analysis with PVDF membrane (Millipore, Bedford, MA) using polyclonal anti-adiponectin[60], C/EBPα, pAkt (Ser473), tAkt, pErk1/2 (Thr202/Tyr204) and tErk1/2 (#8178, #9271, #9272, #9101 and #9102 Cell Signaling, Danvers, MA) and β-actin (Sigma, St. Louis, Mo) antibodies (1:300 dilution for adiponectin, 1:1000 dilution for all other antibodies). For Western blots in Fig. 3b and 3d, Secondary antibodies used were an IRDye 800-coupled goat anti-rabbit secondary antibody (Rockland, Gilbertsville, PA) and an IRDye 700-coupled goat anti mouse secondary antibody (Rockland, Gilbertsville, PA) (for labelling of mouse IgG as serum loading control). The membrane was scanned by the LI-COR Odyssey infrared imaging system at 700- and 800-nm channels simultaneously. For other western blots, ECL method was used and the PVDF membranes were exposed to X-film. All the unprocessed original scans can be found in the Supplementary Fig. 9.

In vivo insulin signaling assay

In vivo insulin signaling in the adipose tissue and liver is measured as described[61]. Briefly, mice were fasted for 24 hours before insulin injection. Anesthetized mice were opened, one side of the two sWATs and eWATs and a piece of liver were excised and snap-frozen in liquid nitrogen for use as untreated control. Four to five min after injection via the portal vein with 1 U/kg of human insulin (Eli Lilly, Indianapolis, Indiana, USA), the other side of sWAT and eWAT and a piece of liver were snap-frozen for subsequent protein extraction and Western immunoblot analysis.

Chromatin immunoprecipitation (CHIP) assays

Differentiated adipocytes in 10 cm dishes were cross-linked in 1% formaldehyde for 10 minutes, followed by quenching with 125 mM glycine solution for 5 minutes. After two washes with cold PBS. Nuclear were extracted by first washing cells in 0.25% Triton-X100, 10 mM EDTA, 0.5 mM EGTA, 10 mM HEPES, pH 6.5, and 200 mM NaCl, and then in 1 mM EDTA, 0.5 mM EGTA, 10 mM HEPES, pH 6.5. Nuclei were resuspended in 1.5% SDS, 10 mM EDTA, 50mM Tris.HCl, pH 8.0, 1X protease inhibitor cocktail and lysed by snap freezing. Sonication was performed for Chromatin fragmentation. For immunoprecipitation, anti-C/EBPα antibodies (sc-61 and sc-9314, Santa Cruz Biotechnologies), anti-PPARγ antibodies (sc-7196 and sc-1984, Santa Cruz Biotechnologies), anti-C/EBPβ antibodies (sc-746x and sc-150x, Santa Cruz Biotechnologies) or rabbit IgG control were used in CHIP dilution buffer (16.7 mM Tris-HCl pH 8.1, 167 mM NaCl, 0.01%SDS, 1.1% Triton-X 100). DNA-protein complex was eluted and cross-link were reversed overnight at 65°C. DNA samples were purified by

Qiagen PCR purification kit. For enrichment analysis, real-time quantitative PCR was done with the SYBR Green PCR system (Applied Biosystems, Foster City).

Immunofluorescence staining

Formalin-fixed, paraffin-embedded sections from adipose tissue (n = 2–3 male mice) were blocked in PBST with 5% BSA. Primary antibody used was perilipin (1:500 dilution) (a kind gift of Dr. Andy Greenberg, Tufts University or NB100-60554, NOVUS) and UCP1 (1:250 dilution) (ab10983, Abcam, Cambridge, England); secondary antibodies (1:200 dilution) used were Alexa Fluor 594 Goat anti-Rabbit IgG (H+L), Alexa Fluor 594 Donkey anti-Goat IgG (H+L) and Alexa Fluor 488 Goat anti-Rabbit IgG (H+L) (Invitrogen, Carlsbad, CA). Slides were counterstained with DAPI. Images were acquired using AxioObserver Epifluorescence Microscope (Zeiss, Jena, Germany).

Microarray analysis

Gene expression profiling was performed at the UTSW Genomics and Microarray Core. For each group, total RNA from sWAT of 9–14 mice were pooled into 3 samples (3–5 mice per sample) labeled and hybridized to Illumina MouseWG-6 v2.0 Expression BeadChips (Illumina, Inc., San Diego, CA) according to manufacturer's protocol. Normalization and statistical analysis of gene expression was performed in by GeneSpring GX software (Agilent Technologies, Santa Clara, CA) and differentially expressed genes were identified using moderated t-statistics with an adjusted p-value <0.05. Canonical Pathway Analysis and Comparison Analysis were performed by the IPA Ingenuity software (Ingenuity Systems, Redwood City, CA).

In vivo scanning

For *in vivo* scans, mice were anesthetized by 1% isoflurane inhalation. The whole body (base of the skull, as the spinal canal begins to widen and the distal end of the tibia) of each mouse was scanned at an isotropic voxel size of 93 μm (80 kV, 450 μA, and 100 msec integration time) using the eXplore Locus microcomputer tomography (CT) scanner (GE Healthcare, Princeton, NJ). Selection of the scan energy and voxel size (scanning increment) was based on optimizing the requirements of scanning time and tissue detail and to minimize exposure to radiation. Based on the scan parameters, the estimated radiation exposure was 4 rad (0.04 Gy) for each scan. Three-dimensional images were reconstructed from two-dimensional gray-scale image slices and visualized using Microview Software (GE Healthcare, Princeton, NJ). Density values for soft tissue and bone were calibrated from a phantom (GE Healthcare, Princeton, NJ) containing air bubble, water, and hydroxyl apatite rod. The region of interest (ROI) for each animal was defined based on skeletal landmarks from the gray-scale images.

Lipid quantifications

Sphingolipids were quantified as described previously by LC/ESI/MS/MS using a Shimadzu Nexera X2 UHPLC system coupled to a Shimadzu LCMS-8050 triple quadrupole mass spectrometer[38]. Lipid species were identified based on exact mass and fragmentation patterns, and verified by lipid standards.

Hepatic triglyceride secretion rate and lipoprotein analysis

Hepatic triglyceride secretion rates were determined by measuring the increases in serum triglycerides after inhibition of lipoprotein lipase[62]. Briefly, tyloxapol (Sigma, St. Louis, MO) was injected via tail-vein at 600 mg/kg, a dose that was reported to completely inhibit triglyceride clearance during VLDL secretion experiments. Serum samples were taken from the tail vein every hour for triglyceride analysis. For lipoprotein fractionation analysis, equal volumes of serum samples were pooled (for a total of 0.4 ml) from 6 mice per group. The pooled plasma from each group was subjected to FPLC gel filtration on a Superose 6 10/300 GL FPLC column (Amersham Biosciences, Piscataway, NJ). The fractions (0.5 ml) were collected and total triglycerides and cholesterol levels of each fraction were determined using the Infinity Triglyceride and Cholesterol Kit (Thermo Electron Corporation, Vantaa, Finland).

Mouse muscle injury and recovery

50 μl of 50% v/v glycerol was intramuscularly injected into tibialis anterior muscle of the right leg, while 50 μl of PBS was injected to the left leg[63]. The injection was performed under anesthesia using isoflurane inhalation. Mice were sacrificed 3 weeks after injection and the tibialis anterior muscles were harvested for histology or RNA extraction.

Reproducibility of experiments

For the requirement of C/EBPα or PPARγ during terminal embryonic adipogenesis (Figure 1), there were two independent experiments. For C/EBPα deletion in differentiated SVF (Figure 2), there were three independent experiments. For adiponectin level in the circulation (Figure 3d), there were three independent experiments. For Adn-C/EBPα$^{flox/flox}$ mice fed on a dox high fat diet (Figure 4b), there were three independent experiments. For GTT on Adn-C/EBPα$^{flox/flox}$ mice fed on a dox high fat diet (Figure 4g, h), there were two independent experiments. For *ob/ob* Adn-C/EBPα$^{flox/flox}$ mice fed on a dox chow diet (Figure 5b, c), there were two independent experiments. For *ob/ob* Adn-C/EBPα$^{flox/flox}$ AdTg mice fed on a dox chow diet, there were two independent experiments. For muscle injury in Adn-C/EBPα$^{flox/flox}$ mice (Figure 6g), there were two independent experiments. For cold induced beige adipogenesis in Adn-C/EBPα$^{flox/flox}$ mice (Figure 6g), there were two independent experiments. For tissue profile of C/EBPa knockdown (Supplementary Fig. 1b), there were two independent experiments. For fat floating (Supplementary Fig. 1c), there were two independent experiments. For Triglyceride content of the VLDL fractions and cholesterol content of the HDL fractions (Supplementary Fig. 5a, b), there were two independent experiments. For the rest of results shown in figures, there was no replication of mouse experiments. There is no estimate of variation in each group of data and the variance is similar between the groups. No statistical method was used to predetermine sample size. The experiments were not randomized. The Investigators were not blinded to allocation during experiments and outcome assessment. All data is expected to have normal distribution.

Statistical analysis

Data are presented as means ± s.e.m. Differences were analyzed by unpaired two-tailed t -test between two groups or otherwise by two-way ANOVA.

Microarray data accession

The Microarray data is deposited in GEO (accession code GSE62937, link: http://www.ncbi.nlm.nih.gov/geo/query/acc.cgi?acc=GSE62937).

Supplementary Material

Refer to Web version on PubMed Central for supplementary material.

Acknowledgments

We thank the UT Southwestern Histology Core for assistance in imbedding and processing of tissue samples. This study was supported by US National Institutes of Health (NIH) grants R01-DK55758, P01-DK088761 and R01-DK099110 (P.E.S.). Q.A.W. is supported by a postdoctoral fellowship from the American Diabetes Association (7-11-MN-47). R.K.G. is supported by NIH grant R03-DK099428 and the Searle Scholars Program (Chicago, Illinois).

References

1. Scherer PE. Adipose tissue: from lipid storage compartment to endocrine organ. Diabetes. 2006; 55:1537–1545. [PubMed: 16731815]
2. Rosen ED, Spiegelman BM. Adipocytes as regulators of energy balance and glucose homeostasis. Nature. 2006; 444:847–853. [PubMed: 17167472]
3. Cinti S. The adipose organ at a glance. Disease Models & Mechanisms. 2012; 5:588–594. [PubMed: 22915020]
4. Abate N, Garg A, Peshock R, Stray-Gunderson J, Grundy S. Relationship of generalized and original adiposity to insulin sensitivity in men. J Clin Invest. 1995; 96:88–98. [PubMed: 7615840]
5. Miyazaki Y, DeFronzo R. Visceral fat dominant distribution in male type 2 diabetic patients is closely related to hepatic insulin resistance, irrespective of body type. Cardiovascular Diabetology. 2009; 8:44. [PubMed: 19656356]
6. McLaughlin T, Lamendola C, Liu A, Abbasi F. Preferential Fat Deposition in Subcutaneous Versus Visceral Depots Is Associated with Insulin Sensitivity. Journal of Clinical Endocrinology & Metabolism. 2011; 96:E1756–E1760. [PubMed: 21865361]
7. Gesta S, Tseng YH, Kahn CR. Developmental Origin of Fat: Tracking Obesity to Its Source. Cell. 2007; 131:242–256. [PubMed: 17956727]
8. Cristancho AG, Lazar MA. Forming functional fat: a growing understanding of adipocyte differentiation. Nat Rev Mol Cell Biol. 2011; 12:722–734. [PubMed: 21952300]
9. Spiegelman BM, Flier JS. Obesity and the regulation of energy balance. Cell. 2001; 104:531–543. [PubMed: 11239410]
10. Mikkelsen TS, et al. Comparative Epigenomic Analysis of Murine and Human Adipogenesis. Cell. 2010; 143:156–169. [PubMed: 20887899]
11. Farmer SR. Transcriptional control of adipocyte formation. Cell Metabolism. 2006; 4:263–273. [PubMed: 17011499]
12. Rosen ED, MacDougald OA. Adipocyte differentiation from the inside out. Nat Rev Mol Cell Biol. 2006; 7:885–896. [PubMed: 17139329]
13. Lefterova MI, et al. PPARgamma and C/EBP factors orchestrate adipocyte biology via adjacent binding on a genome-wide scale. Genes & development. 2008; 22:2941–2952. [PubMed: 18981473]

14. Nielsen R, et al. Genome-wide profiling of PPARgamma:RXR and RNA polymerase II occupancy reveals temporal activation of distinct metabolic pathways and changes in RXR dimer composition during adipogenesis. Genes & development. 2008; 22:2953–2967. [PubMed: 18981474]
15. Rosen, Evan D.; Spiegelman, Bruce M. What We Talk About When We Talk About Fat. Cell. 2014; 156:20–44. [PubMed: 24439368]
16. Berry R, Rodeheffer MS. Characterization of the adipocyte cellular lineage in vivo. Nature cell biology. 2013; 15:302–308. [PubMed: 23434825]
17. Gupta RK, et al. Transcriptional control of preadipocyte determination by Zfp423. Nature. 2010; 464:619–623. [PubMed: 20200519]
18. Jeffery E, Church CD, Holtrup B, Colman L, Rodeheffer MS. Rapid depot-specific activation of adipocyte precursor cells at the onset of obesity. Nature cell biology. 2015; 17:376–385. [PubMed: 25730471]
19. Berry R, Jeffery E, Rodeheffer Matthew S. Weighing in on Adipocyte Precursors. Cell Metabolism. 2014; 19:8–20. [PubMed: 24239569]
20. Wang ZV, Deng Y, Wang QA, Sun K, Scherer PE. Identification and characterization of a promoter cassette conferring adipocyte-specific gene expression. Endocrinology. 2010; 151:2933–2939. [PubMed: 20363877]
21. Sun K, et al. Dichotomous effects of VEGF-A on adipose tissue dysfunction. Proceedings of the National Academy of Sciences. 2012; 109:5874–5879.
22. Perl AK, Wert SE, Nagy A, Lobe CG, Whitsett JA. Early restriction of peripheral and proximal cell lineages during formation of the lung. Proceedings of the National Academy of Sciences of the United States of America. 2002; 99:10482–10487. [PubMed: 12145322]
23. Zhang P, et al. Enhancement of hematopoietic stem cell repopulating capacity and self-renewal in the absence of the transcription factor C/EBP alpha. Immunity. 2004; 21:853–863. [PubMed: 15589173]
24. Wu Z, Xie Y, Bucher N, Farmer SR. Conditional ectopic expression of C/EBP beta in NIH-3T3 cells induces PPAR gamma and stimulates adipogenesis. Genes & development. 1995; 9:2350–2363. [PubMed: 7557387]
25. Hamm JK, Park BH, Farmer SR. A role for C/EBPbeta in regulating peroxisome proliferator-activated receptor gamma activity during adipogenesis in 3T3-L1 preadipocytes. The Journal of biological chemistry. 2001; 276:18464–18471. [PubMed: 11279134]
26. Rosen ED, et al. C/EBPα induces adipogenesis through PPARγ: a unified pathway. Genes & development. 2002; 16:22–26. [PubMed: 11782441]
27. Wu Z, et al. Cross-regulation of C/EBPα and PPARγ controls the transcriptional pathway of adipogenesis and insulin sensitivity. Molecular cell. 1999; 3:151–158. [PubMed: 10078198]
28. Linhart HG, et al. C/EBPα is required for differentiation of white, but not brown, adipose tissue. Proceedings of the National Academy of Sciences. 2001; 98:12532–12537.
29. Wang ND, et al. Impaired energy homeostasis in C/EBP alpha knockout mice. Science (New York, NY). 1995; 269:1108–1112.
30. Chatterjee R, et al. Suppression of the C/EBP family of transcription factors in adipose tissue causes lipodystrophy. Journal of Molecular Endocrinology. 2011; 46:175–192. [PubMed: 21321096]
31. Wang QA, Tao C, Gupta RK, Scherer PE. Tracking adipogenesis during white adipose tissue development, expansion and regeneration. Nature medicine. 2013; 19:1338–1344.
32. He W, et al. Adipose-specific peroxisome proliferator-activated receptor γ knockout causes insulin resistance in fat and liver but not in muscle. Proceedings of the National Academy of Sciences. 2003; 100:15712–15717.
33. Wang F, Mullican SE, DiSpirito JR, Peed LC, Lazar MA. Lipoatrophy and severe metabolic disturbance in mice with fat-specific deletion of PPARγ. Proceedings of the National Academy of Sciences. 2013; 110:18656–18661.
34. Imai T, et al. Peroxisome proliferator-activated receptor γ is required in mature white and brown adipocytes for their survival in the mouse. Proceedings of the National Academy of Sciences of the United States of America. 2004; 101:4543–4547. [PubMed: 15070754]

35. He W, et al. Adipose-specific peroxisome proliferator-activated receptor gamma knockout causes insulin resistance in fat and liver but not in muscle. Proceedings of the National Academy of Sciences of the United States of America. 2003; 100:15712–15717. [PubMed: 14660788]
36. Yang J, et al. Metabolic Response of Mice to a Postnatal Ablation of CCAAT/Enhancer-binding Protein α. Journal of Biological Chemistry. 2005; 280:38689–38699. [PubMed: 16166091]
37. Holland WL, Summers SA. Sphingolipids, insulin resistance, and metabolic disease: new insights from in vivo manipulation of sphingolipid metabolism. Endocrine reviews. 2008; 29:381–402. [PubMed: 18451260]
38. Holland WL, et al. Receptor-mediated activation of ceramidase activity initiates the pleiotropic actions of adiponectin. Nature medicine. 2010; 17:55–63.
39. Wang QA, Scherer PE, Gupta RK. Improved methodologies for the study of adipose biology: insights gained and opportunities ahead. Journal of Lipid Research. 2014; 55:605–624. [PubMed: 24532650]
40. Kim JY, et al. Obesity-associated improvements in metabolic profile through expansion of adipose tissue. The Journal of Clinical Investigation. 2007; 117:2621–2637. [PubMed: 17717599]
41. Pajvani UB, et al. Fat apoptosis through targeted activation of caspase 8: a new mouse model of inducible and reversible lipoatrophy. Nat Med. 2005; 11:797–803. [PubMed: 15965483]
42. Joe AW, et al. Muscle injury activates resident fibro/adipogenic progenitors that facilitate myogenesis. Nature cell biology. 2010; 12:153–163. [PubMed: 20081841]
43. Harms M, Seale P. Brown and beige fat: development, function and therapeutic potential. Nat Med. 2013; 19:1252–1263. [PubMed: 24100998]
44. Wu J, et al. Beige adipocytes are a distinct type of thermogenic fat cell in mouse and human. Cell. 2012; 150:366–376. [PubMed: 22796012]
45. Wu J, et al. Beige Adipocytes Are a Distinct Type of Thermogenic Fat Cell in Mouse and Human. Cell. 150:366–376. [PubMed: 22796012]
46. Chau YY, et al. Visceral and subcutaneous fat have different origins and evidence supports a mesothelial source. Nature cell biology. 2014; 16:367–375. [PubMed: 24609269]
47. Sanchez-Gurmaches J, Guertin DA. Adipocytes arise from multiple lineages that are heterogeneously and dynamically distributed. Nature communications. 2014; 5:4099.
48. Macotela Y, et al. Intrinsic Differences in Adipocyte Precursor Cells From Different White Fat Depots. Diabetes. 2012; 61:1691–1699. [PubMed: 22596050]
49. Tchkonia T, et al. Mechanisms and Metabolic Implications of Regional Differences among Fat Depots. Cell Metabolism. 2013; 17:644–656. [PubMed: 23583168]
50. Baglioni S, et al. Functional Differences in Visceral and Subcutaneous Fat Pads Originate from Differences in the Adipose Stem Cell. PLoS ONE. 2012; 7:e36569. [PubMed: 22574183]
51. Park SK, et al. CCAAT/enhancer binding protein and nuclear factor-Y regulate adiponectin gene expression in adipose tissue. Diabetes. 2004; 53:2757–2766. [PubMed: 15504955]
52. Qiao L, et al. C/EBPalpha regulates human adiponectin gene transcription through an intronic enhancer. Diabetes. 2005; 54:1744–1754. [PubMed: 15919796]
53. Qiao L, Schaack J, Shao J. Suppression of adiponectin gene expression by histone deacetylase inhibitor valproic acid. Endocrinology. 2006; 147:865–874. [PubMed: 16282359]
54. Maeda N, et al. Diet-induced insulin resistance in mice lacking adiponectin/ACRP30. Nat Med. 2002; 8:731–737. [PubMed: 12068289]
55. Kusminski CM, et al. MitoNEET-driven alterations in adipocyte mitochondrial activity reveal a crucial adaptive process that preserves insulin sensitivity in obesity. Nat Med. 2012; 18:1539–1549. [PubMed: 22961109]
56. Ye R, et al. Adiponectin is essential for lipid homeostasis and survival under insulin deficiency and promotes beta-cell regeneration. Elife. 2014; 3
57. Ye R, Scherer PE. Adiponectin, driver or passenger on the road to insulin sensitivity? Mol Metab. 2013; 2:133–141. [PubMed: 24049728]
58. Asterholm IW, Scherer PE. Enhanced metabolic flexibility associated with elevated adiponectin levels. Am J Pathol. 2010; 176:1364–1376. [PubMed: 20093494]

59. Shetty S, Kusminski CM, Scherer PE. Adiponectin in health and disease: evaluation of adiponectin-targeted drug development strategies. Trends Pharmacol Sci. 2009; 30:234–239. [PubMed: 19359049]

60. Scherer PE, Williams S, Fogliano M, Baldini G, Lodish HF. A Novel Serum Protein Similar to C1q, Produced Exclusively in Adipocytes. Journal of Biological Chemistry. 1995; 270:26746–26749. [PubMed: 7592907]

61. Wang Q, et al. Abrogation of hepatic ATP-citrate lyase protects against fatty liver and ameliorates hyperglycemia in leptin receptor-deficient mice. Hepatology. 2009; 49:1166–1175. [PubMed: 19177596]

62. Wang Q, et al. Deficiency in hepatic ATP-citrate lyase affects VLDL-triglyceride mobilization and liver fatty acid composition in mice. Journal of Lipid Research. 2010; 51:2516–2526. [PubMed: 20488800]

63. Lukjanenko L, Brachat S, Pierrel E, Lach-Trifilieff E, Feige JN. Genomic profiling reveals that transient adipogenic activation is a hallmark of mouse models of skeletal muscle regeneration. PLoS One. 2013; 8:e71084. [PubMed: 23976982]

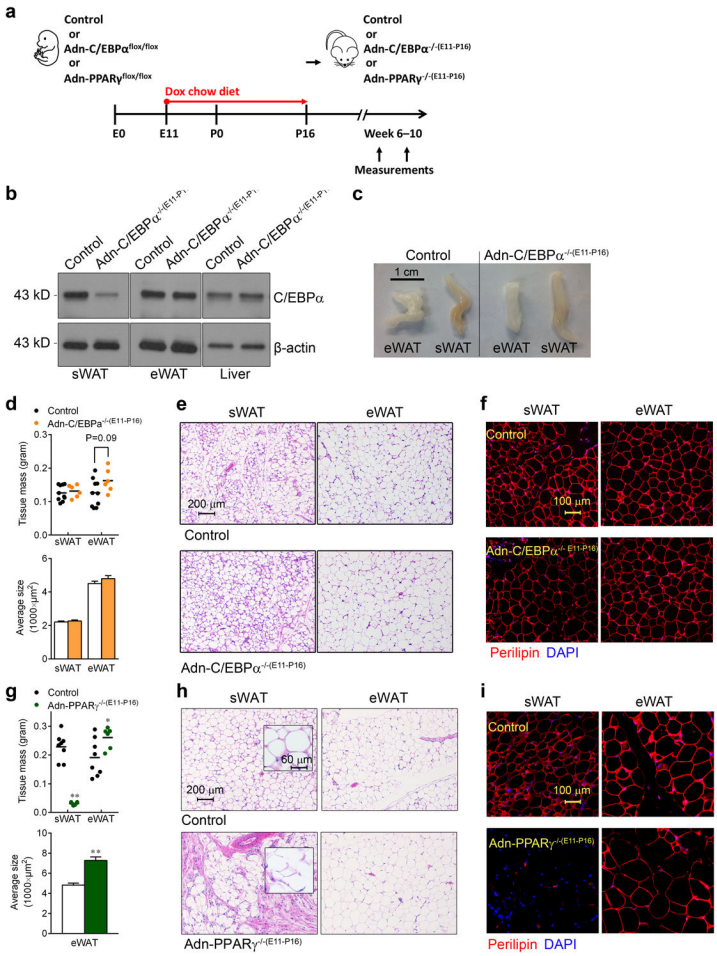

Figure 1. C/EBPα is not required for terminal embryonic adipogenesis

a. Experimental design: Adn-C/EBPα$^{flox/flox}$ or control littermates (mice contains only Adn-rtTA and C/EBPα$^{flox/flox}$) of both genders, Adn-PPARγ$^{flox/flox}$ male mice and control littermates (mice carrying only Adn-rtTA and PPARγ$^{flox/flox}$) were on doxycycline (dox) chow diet during E11–P16. After P16, they were switched to normal chow diet to generate Adn-C/EBPα$^{-/-(E11\text{-}P16)}$ or Adn-PPARγ$^{-/-(E11\text{-}P16)}$ mice.

b. Western-blot of C/EBPα levels in protein extracts of sWAT, eWAT and liver from Adn-C/EBPα$^{-/-(E11\text{-}P16)}$ male mice and their control male littermates at 7 weeks of age. 2 male mice per group. These images are from a single Western-blot experiment.

c. Whole tissue pictures of eWAT and sWAT from Adn-C/EBPα$^{-/-(E11\text{-}P16)}$ male mice and their control male littermates at 7 weeks of age. These images are from a single experiment.

d. sWAT and eWAT tissue mass (top) and average adipocyte size (bottom) of Adn-C/EBPα$^{-/-(E11\text{-}P16)}$ male mice and their control male littermates at 7 weeks of age. For adipose tissue mass, n = 5 male mice (10 fat depots, control group), n = 3 male mice (6 fat depots, Adn-C/EBPα$^{-/-(E11\text{-}P16)}$ group). This experiment is representative of two independent experiments. For adipocyte size, n = 339 cells (control, sWAT); 408 cells (Adn-C/EBPα$^{-/-(E11\text{-}P16)}$, sWAT); 338 cells (control, eWAT); 323 cells (Adn-C/EBPα$^{-/-(E11\text{-}P16)}$, eWAT). Data represent the mean ± s.e.m. Student's t-test. This data is from a single experiment.

e, f. H&E staining (**e**) and perilipin (red)/DAPI (blue) immunofluorescence staining (**f**) in sWAT and eWAT in Adn-C/EBPα$^{-/-(E11\text{-}P16)}$ male mice and their control male littermates. These images are representative of two independent experiments.

g. sWAT and eWAT tissue mass (top) and average adipocyte size (bottom) of Adn-PPARγ$^{-/-(E11\text{-}P16)}$ male mice and their control male littermates were measured when they were 10 weeks of old. For tissue mass, $n = 4$ male mice (8 fat depots, control group), $n = 3$ male mice (6 fat depots, Adn- PPARγ$^{-/-(E11\text{-}P16)}$ group). **, $P < 0.001$ for sWAT; *, $P = 0.04$ for eWAT. This experiment is representative of two independent experiments. For average adipocyte size, $n = 335$ cells (control, eWAT); 245 cells (Adn- PPARγ$^{-/-(E11\text{-}P16)}$, eWAT. **, $P < 0.001$. All compared to control group. All data represent the mean ± s.e.m. Student's t-test.

h, i. H&E (**h**) and perilipin (red)/DAPI (blue) immunofluorescence staining (**i**) shows the adipocyte morphology in sWAT and eWAT of Adn-PPARγ$^{-/-(E11\text{-}P16)}$ male mice, compared to their control male littermates. These image are representative of two independent experiments.

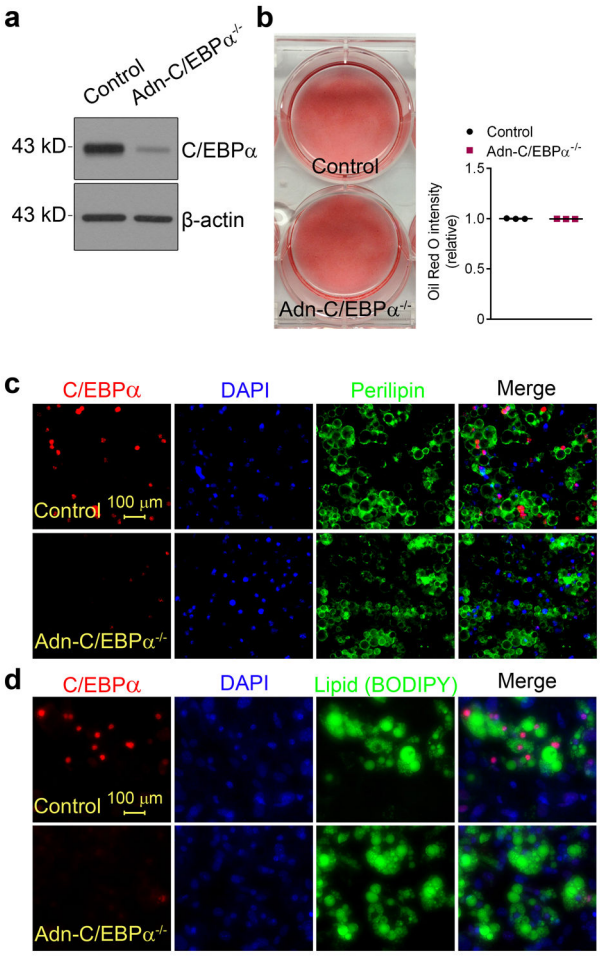

Figure 2. C/EBPα deficient adipocytes are viable and have normal lipid accumulation *in vitro*

a. Western-blots of C/EBPα in protein extracts of differentiated adipocytes from SVF of Adn-C/EBPα$^{flox/flox}$ mice or control littermates, treated with doxycycline for 3 days. These images are representative of two independent Western-blot experiments.

b. Oil red O staining on differentiated adipocytes from SVF of Adn-C/EBPα$^{flox/flox}$ mice or control littermates, treated with doxycycline for 3 days (left). Relative Oil Red O intensity was measured by ImageJ software (right). *n* = 3 wells of a six-well plate for each group. This experiment is representative of three independent experiments.

c, d. immunofluorescence stains for C/EBPα (red), DAPI (blue) and perilipin (green) (**c**) or C/EBPα (red), DAPI (blue) and BODIPY (green) (**d**) on differentiated adipocytes treated with doxycycline for 3 days. These images are representative of two independent experiments.

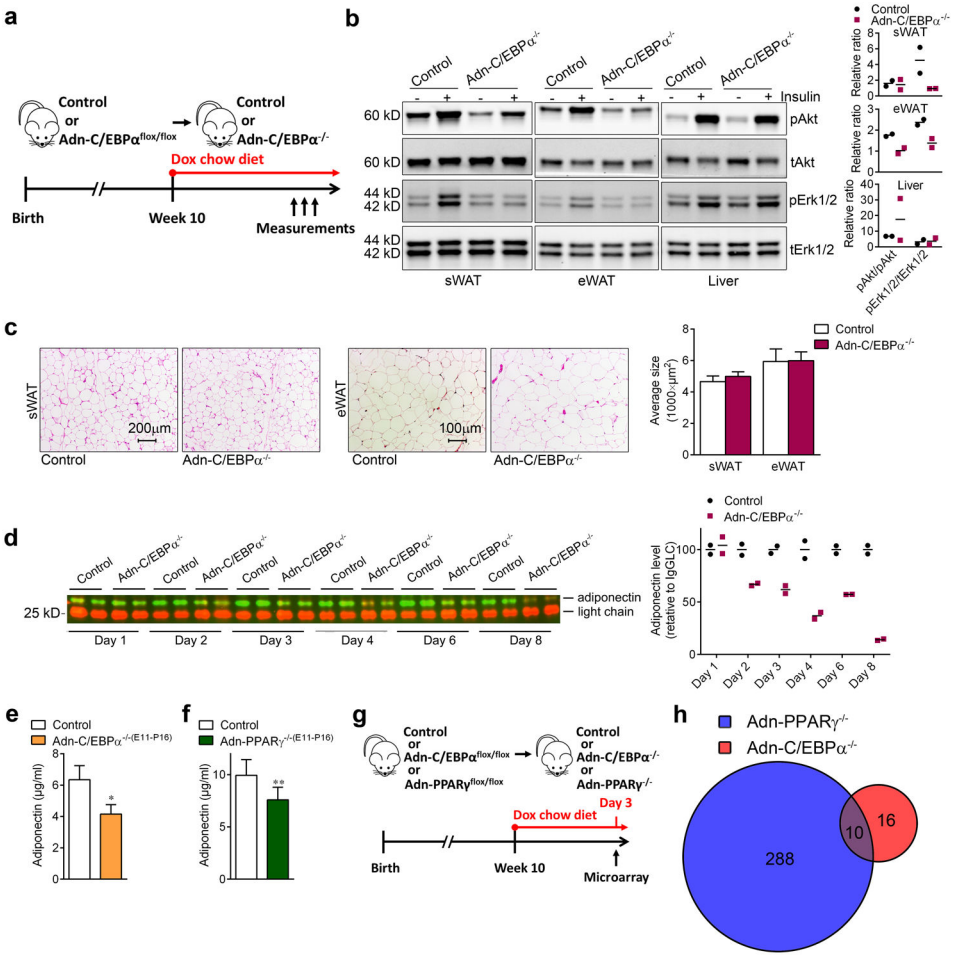

Figure 3. Normal viability and lipid accumulation in inducible C/EBPα deficient adipocytes *in vivo*

a. Experimental design: Adn-C/EBPα$^{flox/flox}$ mice started doxycycline chow diet treatment on 10 weeks of age to generate Adn-C/EBPα$^{-/-}$ mice.

b. Western-blots of phospho-Akt (Ser473), total Akt, phospho-Erk1/2 (Thr202/Tyr204) and total Erk1/2 levels in protein extracts of sWAT, eWAT and liver from Adn-C/EBPα$^{-/-}$ mice and their control littermates after 4 days of doxycycline chow diet feeding. *n* = 2 male mice per group. The bar graphs indicate the fold stimulation of pAkt and pErk1/2 phosphorylation relative to tAkt and tErk1/2. Data represent the mean. These images are representative of two independent Western-blot experiments.

c. H&E staining (left) and average adipocyte size (right) in sWAT and eWAT of both groups after 1 month of doxycycline HFD feeding. These images are representative of two independent experiments. For adipocyte sizes, *n* = 154 cells (control, sWAT); 192 cells (Adn-C/EBPα$^{-/-}$, sWAT); 76 cells (control, eWAT); 86 cells (Adn-C/EBPα$^{-/-}$, eWAT). All data represent the mean ± s.e.m.. All from one image shown in the figure. This data is from a single experiment.

d. Western-blot of circulating adiponectin after 1–8 days of doxycycline chow diet feeding and quantification (left). Relative protein levels were determined by densitometry quantification of the immunoblots after normalization to IgG light chain (LgGLC) (right). *n*

= 2 male mice per group. Data represent the mean. Theses image is representative of three independent Western-blot experiments.

e, f. Circulating adiponectin levels tested by ELISA in Adn-C/EBPα$^{-/-(E11\text{-}P16)}$ male mice (**e**), Adn-PPARγ$^{-/-(E11\text{-}P16)}$ male mice (**f**) and their control male littermates at 8 weeks of age. *n* = 5 male mice (control group for both e and f), *n* = 3 male mice (Adn-C/EBPα$^{-/-(E11\text{-}P16)}$ group), *n* = 9 male mice (Adn-PPARγ$^{-/-(E11\text{-}P16)}$ group). *, *P* = 0.01 for Adn-C/EBPα$^{-/-(E11\text{-}P16)}$ mice; **, *P* = 0.008 for Adn-PPARγ$^{-/-(E11\text{-}P16)}$ mice. All data represent the mean ± s.e.m. Student's t-test.

g. Experimental design: for microarray analysis, 10 weeks old Adn-C/EBPα$^{flox/flox}$ male mice or Adn-PPARγ$^{flox/flox}$ male mice and their control male littermates were kept on doxycycline chow diet for 3 days to generate Adn-C/EBPα$^{-/-}$ or Adn-PPARγ$^{-/-}$ mice. *n* = 14, control group for Adn-PPARγ$^{-/-}$; *n* = 10, Adn-PPARγ$^{-/-}$ group and control group for Adn-C/EBPα$^{-/-}$; *n* = 12, Adn-C/EBPα$^{-/-}$ group.

h. Overlap of C/EBPα direct responsive genes and PPARγ direct responsive genes. *P* cut-off: 0.05; fold change cut-off: 1.5. Student's t-test. This data is from a single experiment.

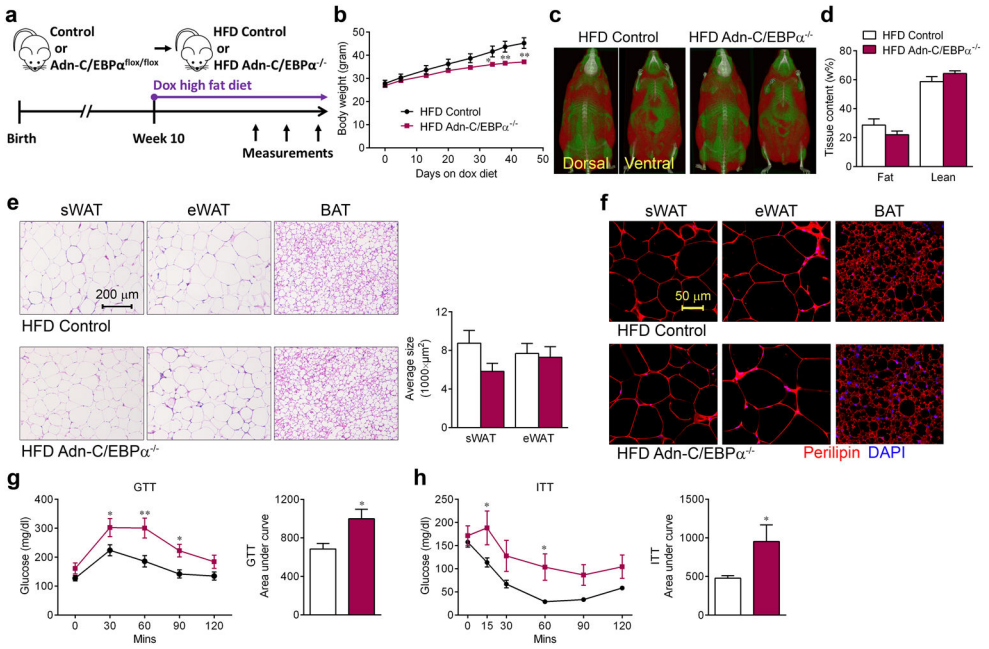

Figure 4. Mice with inducible C/EBPα elimination in adipocytes have impaired glucose and lipid metabolism during high fat diet challenge

a. Experimental design: Adn-C/EBPα$^{flox/flox}$ mice started doxycycline (dox) HFD treatment at10 weeks of age to generate HFD Adn-C/EBPα$^{-/-}$ mice.

b. Body weights of both groups during doxycycline HFD feeding. *n* = 6 male mice (HFD control group), *n* = 11 male mice (HFD Adn-C/EBPα$^{-/-}$ group). *, *P* = 0.02 at day 34; **, *P* <0.001 at day 38; **, *P* <0.001 at day 44, compared to HFD control group. Data represent the mean ± s.e.m. Student's t-test. This experiment is representative of three independent experiments.

c. Magnetic resonance imaging analysis of both groups after 4 weeks of doxycycline HFD feeding. Red mass represents adipose tissue. These images are from a single experiment.

d. NMR body fat and lean content of both groups after 4 weeks of doxycycline HFD feeding. *n* = 11 male mice per group. Data represent the mean ± s.e.m. This data is from a single experiment.

e. H&E staining (left) in sWAT, eWAT and BAT and average adipocyte size (right) of sWAT and eWAT, as indicated, of both groups after 4 weeks of doxycycline HFD feeding. These images are representative of two independent experiments. For adipocyte sizes, *n* = 53 cells (HFD control, sWAT); 42 cells (HFD Adn-C/EBPα$^{-/-}$, sWAT); 43 cells (HFD control, eWAT); 47 cells (HFD Adn-C/EBPα$^{-/-}$, eWAT). All data represent the mean ± s.e.m. Student's t-test. All from one image shown in the figure. This data is from a single experiment.

f. Immunofluorescence staining for perilipin (red) and DAPI (blue) in sWAT, eWAT and BAT, as indicated, of both groups after 4 weeks of doxycycline HFD feeding. This image is representative of two independent experiments.

g, h. GTT (**f**) and ITT (**g**) were performed during the 4th and 6th week of doxycycline HFD feeding on Adn-C/EBPα$^{-/-}$ mice and their control littermates, the bar graph represents the area under the curve. For GTT, *n* = 10 male mice (HFD control group), *n* = 8 male mice

(HFD Adn-C/EBPα$^{-/-}$ group). For ITT, n = 7 male mice (HFD control group), n = 6 male mice (HFD Adn-C/EBPα$^{-/-}$ group). *, P = 0.047, 0.039 for GTT 30, 90 minutes; **, P = 0.001 for GTT 60 minutes; *, P = 0.01 for GTT AUC; *, P = 0.048 for ITT 15, 60 minutes, *, P = 0.04 for ITT AUC, compared to HFD control group. All data represent the mean ± s.e.m. Two-way ANOVA. These experiment are all representative of two independent experiments.

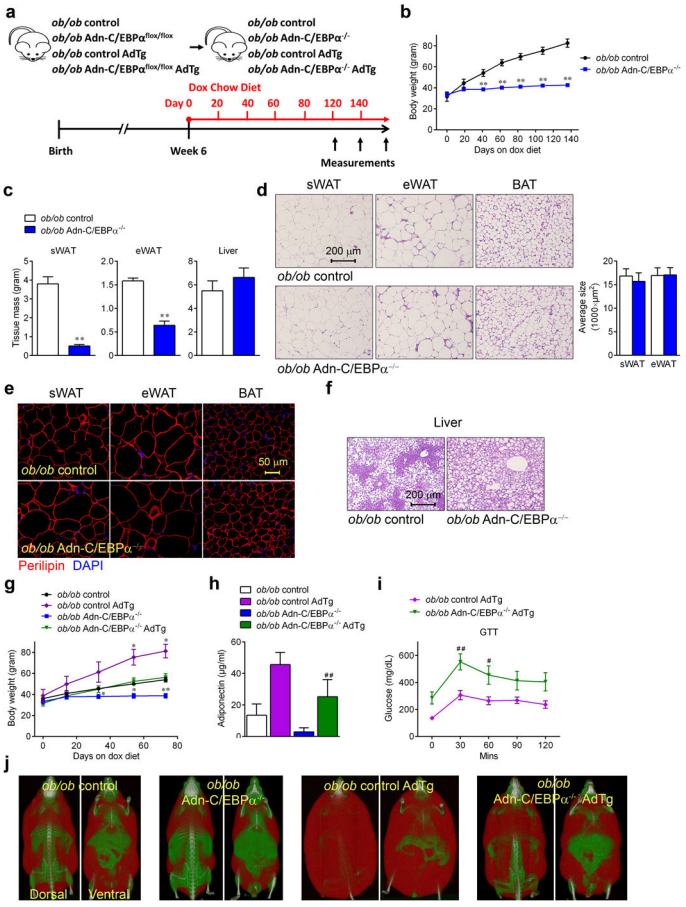

Figure 5. Inducible deletion of C/EBPα in adipocytes of *ob/ob* mice attenuates adipose tissue expansion, which can be rescued by adiponectin overexpression

a. Experimental design: *ob/ob* Adn-C/EBPα$^{flox/flox}$ mice or *ob/ob* Adn-C/EBPα$^{flox/flox}$ AdTg mice started doxycycline chow diet treatment at 6 weeks of age to generate *ob/ob* Adn-C/EBPα$^{-/-}$ mice or *ob/ob* Adn-C/EBPα$^{-/-}$ AdTg mice.

b. Body weights during doxycycline chow diet feeding. n = 5 male mice per group. **, P <0.001 at day 41, 62, 83, 108 and 136. Student's t-test. This experiment is representative of two independent experiments. **c.** sWAT, eWAT and liver tissue weight. n = 5 male mice per group. **, P <0.001, compared to *ob/ob* control group. Student's t-test. This experiment is representative of two independent experiments.

d. H&E staining (left) of sWAT, eWAT and BAT, and average adipocyte size (right) of sWAT and eWAT, as indicated. These images are representative of two independent experiments. For adipocyte sizes, n = 105 cells (*ob/ob* control, sWAT); 60 cells (*ob/ob* Adn-C/EBPα$^{-/-}$, sWAT); 80 cells (*ob/ob* control, eWAT); 89 cells (*ob/ob* Adn-C/EBPα$^{-/-}$, eWAT). All data represent the mean ± s.e.m. Student's t-test. All from one image shown in the figure. This data is from a single experiment..

e. Immunofluorescence staining for perilipin (red) and DAPI (blue) in sWAT, eWAT and BAT. These images are representative of two independent experiments.

f. H&E staining of liver. These images are representative of two independent experiments.

g. Body weights during doxycycline chow diet feeding. *n* = 3 male mice (*ob/ob* control group, *ob/ob* control AdTg group and *ob/ob* Adn-C/EBPα$^{-/-}$ group), *n* = 7 male mice (*ob/ob* Adn-C/EBPα$^{-/-}$ AdTg group). *, *P* = 0.03, 0.02 at day 54 and 73 for *ob/ob* control AdTg compared to *ob/ob* control group. *, *P* = 0.03, 0.01 at day 33 and 54; **, *P* <0.001 at day 73 for *ob/ob* Adn-C/EBPα$^{-/-}$ compared to *ob/ob* control group. Data represent the mean ± s.e.m. Student's t-test. This experiment is representative of two independent experiments.
h. Circulating adiponectin levels tested by ELISA. *n* = 2 male mice (*ob/ob* control group), *n* = 8 male mice (*ob/ob* control AdTg group), *n* = 5 male mice (*ob/ob* Adn-C/EBPα$^{-/-}$ group), *n* = 6 male mice (*ob/ob* Adn-C/EBPα$^{-/-}$ AdTg group). ##, *P* <0.001 compared to *ob/ob* control AdTg group. Data represent the mean ± s.e.m. Student's t-test. This data is from a single experiment.
i. GTT performed during the 10th week of doxycycline chow diet. *n* = 13 male mice (*ob/ob* control AdTg group), *n* = 12 male mice (*ob/ob* Adn-C/EBPα$^{-/-}$ AdTg group). *, *P* = 0.02, at 60 minutes; **, *P* = 0.001 at 30 minutes compared to *ob/ob* control AdTg group. Data represent the mean ± s.e.m. Two-way ANOVA. This data is from a single experiment.
j. Magnetic resonance imaging analysis at the 8th week of doxycycline chow diet feeding. These images are from a single experiment.

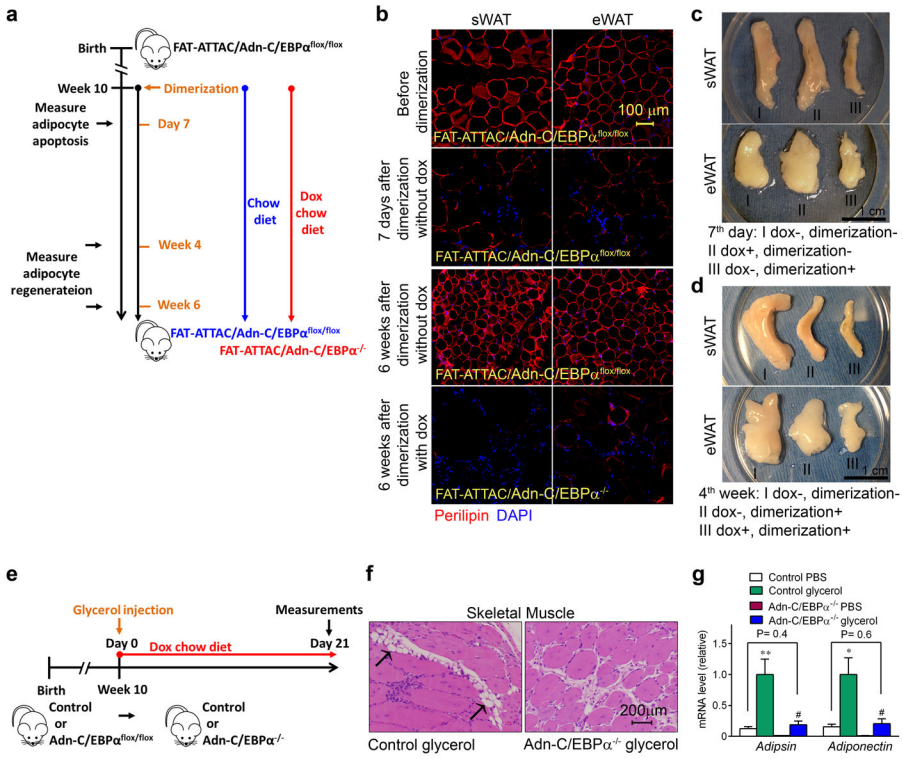

Figure 6. C/EBPα is required for terminal white adipogenesis in the adult stage

a. Experimental design: FAT-ATTAC/Adn-C/EBPα$^{flox/flox}$ mice were kept on chow diet before dimerization. After dimerization at 10 weeks of age, mice were kept on chow diet (FAT-ATTAC/Adn-C/EBPα$^{flox/flox}$) or switched to doxycycline chow diet (FAT-ATTAC/Adn-C/EBPα$^{-/-}$) for up to 6 weeks.

b. Perilipin (red) and DAPI (blue) immunofluorescence staining in sWAT and eWAT of FAT-ATTAC/Adn-C/EBPα$^{flox/flox}$ mice before dimerization, 7 days after dimerization without doxycycline treatment, 6 weeks after dimerization without doxycycline treatment (FAT-ATTAC/Adn-C/EBPα$^{flox/flox}$) or with doxycycline treatment (FAT-ATTAC/Adn-C/EBPα$^{-/-}$). These images are representative of two independent experiments.

c. Whole tissue pictures of sWAT and eWAT of FAT-ATTAC/Adn-C/EBPα$^{flox/flox}$ mice 7 days post dimerization (without doxycycline treatment) (III), compared to FAT-ATTAC/Adn-C/EBPα$^{flox/flox}$ littermate without dimerization and doxycycline treatment (I), or FAT-ATTAC/Adn-C/EBPα$^{-/-}$ littermate with doxycycline treatment (II) but without dimerization. These images are representative of two independent experiments.

d. Whole tissue pictures of sWAT and eWAT of FAT-ATTAC/Adn-C/EBPα$^{flox/flox}$ mice (without dox) (II) and FAT-ATTAC/Adn-C/EBPα$^{-/-}$ littermate (with dox) (III) 4 weeks post dimerization, compared to FAT-ATTAC/Adn-C/EBPα$^{flox/flox}$ littermate without dimerization and doxycycline treatment (I). These images are representative of two independent experiments.

e–g. Experimental design: Adn-C/EBPα$^{flox/flox}$ male mice and their control male littermates at 10 weeks of age were injected with glycerol intramuscularly into the right side of tibialis anterior muscle to induce muscle injury, while PBS was injected to the left side of tibialis anterior muscle as vehicle control (**e**). 3 weeks after glycerol injection, representative H&E

staining shows the tissue morphology and adipocyte (arrows) in tibialis anterior muscles These images are representative of two independent experiments. (**f**). qPCR analysis shows the mRNA expression levels of adipocyte markers *adipsin* and *adiponectin* in muscles injected with PBS or glycerol, both in Adn-C/EBPα$^{-/-}$ mice and their control littermates (**g**). $n = 5$ mice per group. Data represent the mean ± s.e.m. **, $P = 0.008$; *, $P = 0.01$ (adipsin) compared to control PBS group; #, $P = 0.02$; #, $P = 0.04$ (adiponectin) compared to Adn-C/EBPα$^{-/-}$ PBS group. Student's t-test. This experiment is representative of two independent experiments.

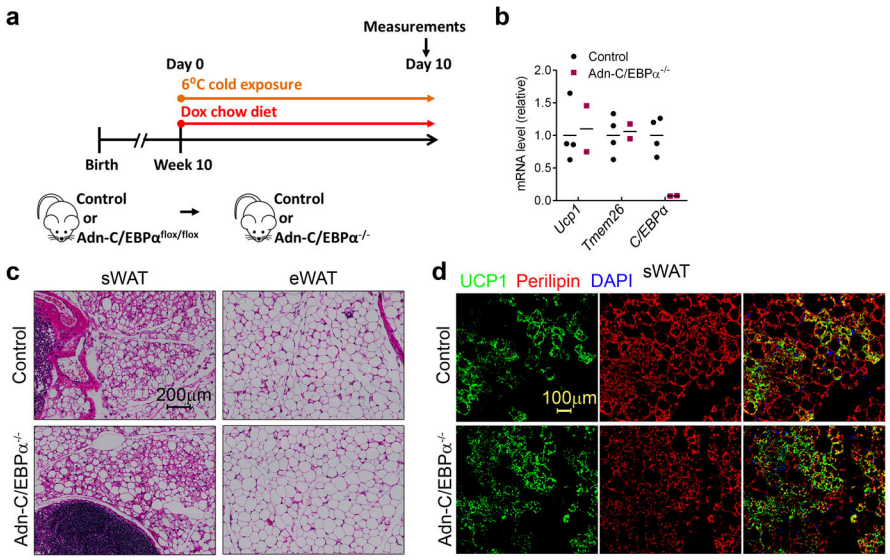

Figure 7. Terminal beige adipogenesis does not depend on C/EBPα

a. Experimental design: Adn-C/EBPα$^{flox/flox}$ male mice and their control male littermates at 10 weeks of age were exposed to cold temperature (6°C) and switched from chow diet to doxycycline chow diet at the same time for 10 days.

b. qPCR analysis shows the mRNA expression levels of beige adipocyte markers *Ucp1* and *Tmem26*, as well as C/EBPα in sWAT of Adn-C/EBPα$^{-/-}$ mice and their control littermates. n = 4 male mice (control group), n = 2 male mice (Adn-C/EBPα$^{-/-}$ group). Data represent the mean. This experiment is representative of two independent experiments.

c, d. H&E staining shows the adipocyte morphology in sWAT and eWAT of both groups (**c**). Immunofluorescence staining shows UCP1 (green), perilipin (red) and DAPI (blue) in sWAT of both groups (**d**). These images are representative of two independent experiments.

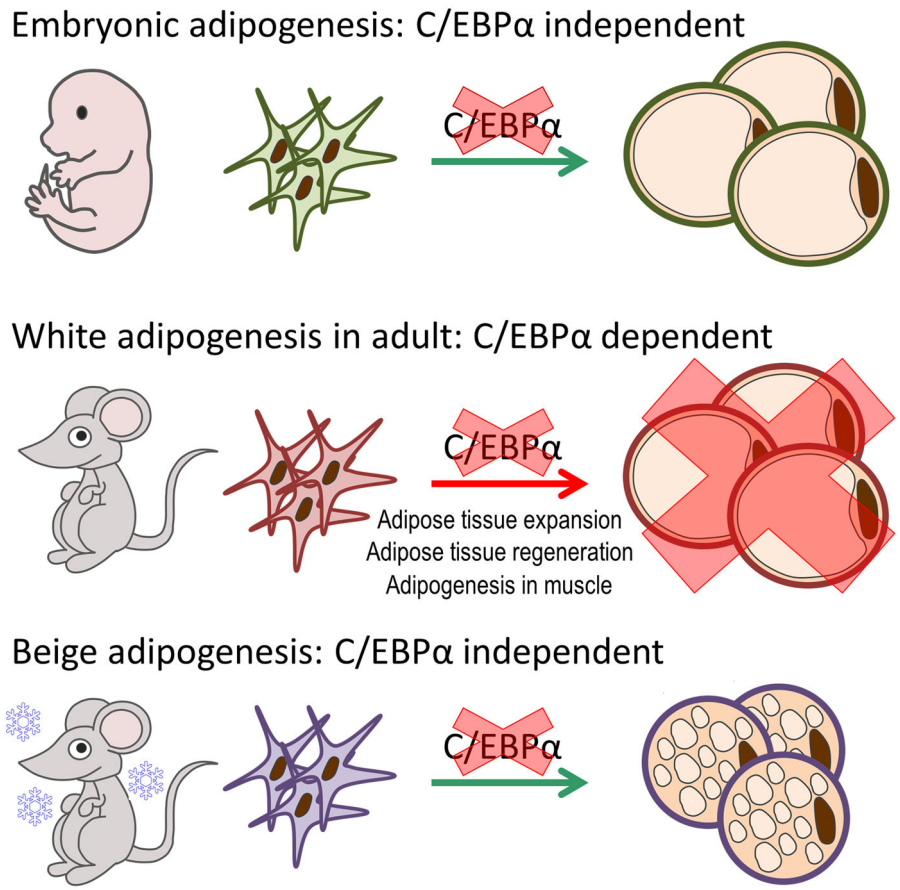

Figure 8. The complexity of adipogenesis *in vivo*

A Schematic summary of the complexity of adipogenesis *in vivo*: C/EBPα is not universally required for all adipogenic conditions. First of all, terminal adipocyte differentiation in sWAT during embryonic development is fully C/EBPα independent. In contrast, C/EBPα is essential for all the terminal white adipogenesis conditions in the adult stage we had tested. These conditions are: adipose tissue expansion during HFD feeding or in leptin deficient mice, regeneration of adipose tissue after ablation and muscle tissue adipogenesis after injury. However, in the adult stage, C/EBPα expression is also not required for cold-induced beige adipogenesis. Our data suggests that white adipocyte precursors in adult animal respond to distinct signals, different from white adipocyte precursors in embryogenesis or beige adipocyte precursors.